J|A|C|S
ARTICLES
Published on Web 02/25/2005

Conformational Analysis of Self-Organized Monolayers with Scanning Tunneling Microscopy at Near-Atomic Resolution

Lukas J. Scherer,[†] Leo Merz,[‡] Edwin C. Constable,*[,†] Catherine E. Housecroft,*[,†] Markus Neuburger,[†] and B. A. Hermann*[,§]

Contribution from the Departments of Chemistry and Physics, University of Basel, Basel, Switzerland, and the Walther-Meissner-Institute (WMI) of Low Temperature Research of the Bavarian Academy of Science and Faculty of Physics/Center for Nano Science (CeNS), LMU Munich, Germany

Received October 20, 2004; E-mail: edwin.constable@unibas.ch; catherine.housecroft@unibas.ch; b.hermann@cens.de

Abstract: We describe the synthesis and a novel approach to the conformational analysis of 2,2′-bipyridines (bpy) bearing aromatic rich Fréchet-type dendritic wedges of the first and second generation as substituents. The evaporation of solutions of these new ligands on graphite surfaces under ambient conditions results in the formation of self-organized monolayers. Scanning tunneling microscopy (STM) investigations of the monolayers under ambient conditions (air, 298 K) gave images at submolecular and near-atomic resolution. The analysis of the STM images includes the following processes: (i) identification and reproduction of potential homoconformational domains, (ii) exclusion of improper data using quality criteria for drift and feedback artifacts, (iii) compilation of running averages and checking for averaging artifacts, (iv) analysis of three-dimensional and contour plots, (v) calculation of the HOMO properties of the free molecules, and (vi) final conformational assignment based on all accessible information. Following this procedure, two different conformations could be assigned to domains observed in the monolayers of the first-generation (G1) and second-generation (G2) dendritic compounds. Homoconformational domains are observed side-by-side. The different conformations arise from syn or anti arrangements at the ether substituents. An additional conformational effect is found upon treating the G1 domains with HCl gas, when a partial rearrangement of the bpy from trans to cis occurs, concomitant with protonation.

Introduction

The direct imaging of species of chemical interest at the molecular and submolecular levels using scanning tunneling and force microscopy has revolutionized possibilities for the visualization and control[1,2] of self-organized systems. Self-assembly and self-organization are increasingly finding application as methodologies for device fabrication, display manufacture, sensor design, and heterogeneous catalyst production.[3] Scanning tunneling microscopy (STM) is an ideal technique for probing self-organized structures, allowing one to investigate molecular orientation and site specificity in a single experiment, and the analysis of a wide range of organic, coordination, and organometallic compounds has been reported.[4−6] Although both static and dynamic properties of these systems have been investigated, the emphasis has generally been upon interactions of molecules within the monolayer and the factors controlling the extended two-dimensional structure that is assembled. However, there is also considerable potential for the study of intramolecular as well as intermolecular structural questions of chemical interest using these new methods. Conventional methods of determining molecular conformation and metrical parameters such as single-crystal X-ray crystallography or NMR spectroscopic methods give structures averaged over some 10^{15} molecules. Analysis of the surface molecular conformation of molecular components within two-dimensional arrays averaged over tens to hundreds of molecules can now be performed by analyzing submolecular-resolved STM images. In other words, it is now becoming possible for the chemist to regard STM as a valid and accessible tool to add to the more conventional methods of determining molecular structure and spatial properties. Here, we report the analysis by STM of a system that exhibits multiple conformers on a graphite surface. We have chosen a 2,2′-bipyridine (bpy) ligand functionalized with Fréchet-type dendrimers of various generations as our core structural unit. STM studies of the parent 2,2′-bipyridine adsorbed on a Au(111) surface have already been reported.[7] The coordination chemistry of bpy ligands is well understood,[8] and coordination to a metal center results in a loss of conformational freedom, locking the ligand in a cis confor-

[†] Department of Chemistry, University of Basel.
[‡] Institute of Physics, University of Basel.
[§] WMI and CeNS, LMU Munich.

(1) Binnig, G.; Rohrer, H. *Helv. Phys. Acta* **1982**, *55*, 726−735.
(2) Binnig, G.; Rohrer, H.; Gerber, C.; Weibel, E. *Phys. Rev. Lett.* **1982**, *49*, 57−61.
(3) Lehn, J.-M. *Supramolecular Chemistry: Concepts and Perspectives*; VCH: Weinheim, Germany, 1995.
(4) De Feyter, S.; De Schryver, F. C. *Chem. Soc. Rev.* **2003**, *32*, 139−150 and references therein.
(5) De Feyter, S.; Gesquière, A.; Abdel-Mottaleb, M. M.; Grim, P. C. M.; De Schryver, F. C.; Meiners, C.; Sieffert, M.; Valiyaveettil, S.; Müllen, K. *Acc. Chem. Res.* **2000**, *33*, 520−531.
(6) Giancarlo L. C.; Flynn, G. W. *Acc. Chem. Res.* **2000**, *33*, 491−501.
(7) Pinheiro, L.S.; Temperini, M. L. A. *Surf. Sci.* **1999**, *441*, 45−52.
(8) Constable, E. C. *Adv. Inorg. Chem. Radiochem.* **1986**, *30*, 69−121.

mation, in contrast to the time-averaged trans conformation in the free ligand.[8,9] This will ultimately allow us to address the conformation of a ligand within a monolayer by reaction with metal salts.[10]

The aromatic-rich system of the Fréchet-type dendrimer[11] is ideally suited for visualization by tunneling methods.[12−16] Additionally, the dendritic compound provides a significant mechanical barrier to rotation about the interannular C−C bond when the conjugates are in a conformationally restricted environment such as in a lattice or in a monolayer on a surface. In this article, we analyze self-organized monolayers of such conjugate structures on surfaces and show that not only one global minimum, but a range of conformations, may be found in surface-bound domains.

Experimental Section

General. Commercially available chemicals were reagent grade and were used without further purification. ^{1}H and ^{13}C NMR spectra were recorded on a Bruker DRX500 spectrometer; δ is relative to TMS, internally referenced to solvent. Infrared spectra were recorded on a Shimadzu FTIR-8400S spectrophotometer with neat samples using a Golden Gate ATR accessory. UV/vis measurements were performed using a Perkin-Elmer Carey 5000 spectrophotometer and were recorded in CH_2Cl_2 solution. Electrospray (ES) mass spectra were recorded on a Bruker Esquire 3000 plus instrument, FAB mass spectra on a Finnegan MAT 312, and MALDI-TOF mass spectra on a Vestec Voyager Elite instrument with α-cyano-4-hydroxycinnamic acid as matrix. The microanalyses were performed with a Leco CHN-900 microanalyzer. 4,4′-Dihydroxy-2,2′-bipyridine[17] and compound **7**[18,19] were prepared by literature methods.

STM. The experiments were carried out in constant current mode using a NanoscopeIII scanning tunneling microscope, equipped with a low current converter. STM tips were mechanically formed from Pt/Ir (9/1) wire. All images were obtained from monolayers on highly oriented pyrolytic graphite (HOPG) substrates. All data used for the analysis were carefully reproduced several times with different tips and different substrate pieces. The data were analyzed using the program SXM-shell (University of Basel, 2004). The 10 nm × 10 nm STM images were prepared by an averaging procedure written for SXM-shell. (Averaging procedures have been used successfully to enhance signal:noise ratios in a wide variety of studies.)[20,21] A sub-image is cut as reference, several similar locations on the original image are found by cross-correlation, and flawed sections are manually deselected. Sub-images cut at the selected places are then averaged into a noise-reduced image. Special care was taken to exclude any averaging artifacts. Individual figure captions state the number of sub-images over which the averaging procedure was carried out. The process of conformational analysis is described in the Results section. Scanning voltages were tried from +1.5 to −1.5 V. The best resolution was obtained between −300 and −1300 mV. We did not observe significant changes in the contrast in this range.

Chart 1

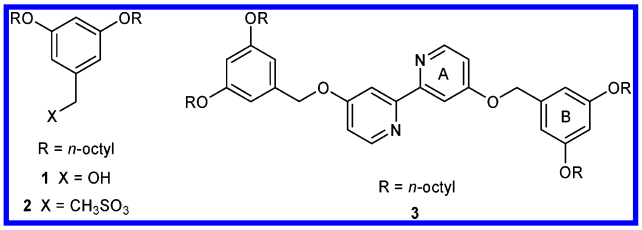

Compound 3. Methanesulfonyl chloride (1.04 mL, 13.5 mmol) was added over 15 min to a mixture of **1** (1.23 g, 3.38 mmol) and NEt_3 (2.08 mL, 16.9 mmol) in dry CH_2Cl_2 (20 mL) at −15 °C under N_2. After being stirred for 1 h at −15 °C, the reaction mixture was poured into a mixture of crushed ice (100 mL) and concentrated HCl (10 mL). The CH_2Cl_2 layer was separated, washed with saturated $NaHCO_3$ solution, dried (Na_2SO_4), and evaporated to give **2** (1.80 g, ca. 80% pure, 3.20 mmol) as an oil. Crude **2** (41.5 mg, ca. 80% pure, 75.0 μmol), 4,4′-dihydroxy-2,2′-bipyridine (6.90 mg, 35.0 μmol), K_2CO_3 (50.0 mg, 362 μmol), and ^{n}Bu$_4$NI (2 mg, 6 μmol) were stirred vigorously in ethyl acetate (400 μL) and water (400 μL) at 60 °C for 20 h. Water (20 mL) was added, and the mixture was extracted three times with ethyl acetate (20 mL). The combined organic layers were dried ($MgSO_4$) and evaporated. Preparative chromatography on silica (CH_2Cl_2/MeOH 10:1) yielded **3** as a white powder (23.1 mg, 26.1 μmol, 74.1%). Chart 1 shows the structures of **1**−**3**. ^{1}H NMR (500 MHz, $CDCl_3$, 25 °C): δ 8.48 (d, J = 5.7 Hz, 2H, H^{6A}), 8.05 (d, J = 2.7 Hz, 2H, H^{3A}), 6.91 (dd, J = 5.7, 2.7 Hz, 2H, H^{5A}), 6.57 (d, J = 2.1 Hz, 4H, H^{2B}), 6.42 (t, J = 2.2 Hz, 2H, H^{4B}), 5.15 (s, 4H, $H^{OCH_2-ringB}$), 3.94 (t, J = 6.6 Hz, 8H, $H^{OCH_2CH_2}$), 1.77 (tt, J = 6.8, 6.5 Hz, 8H, $H^{OCH_2CH_2}$), 1.45 (tt, J = 7.5, 7.3 Hz, 8H, $H^{OCH_2CH_2CH_2}$), 1.25−1.37 (m, 32H, $H^{octyl(CH_2)_4}$), 0.88 (t, J = 7.0 Hz, 12H, H^{CH_3}). ^{13}C NMR (125 MHz, $CDCl_3$, 25 °C): δ 166.1, 160.7, 157.7, 150.4, 138.0, 111.7, 107.5, 105.9, 101.2, 70.1, 68.3, 32.0, 29.5, 29.4 (two overlapping signals), 26.2, 22.8, 14.3. IR (neat): $\bar{\nu}$ (cm^{-1}) 2924 s, 2855 m, 1582 s, 1458 s, 1296 m, 1234 m, 1173 s, 1057 s, 995 s, 833 s. MS (ESI+): m/z 903.5 [M + Na]$^+$, 881.6 [M + H]$^+$; UV/vis (CH_2Cl_2): λ/nm (ϵ/M^{-1} cm^{-1}) 274 (22 400). Anal. Calcd for $C_{56}H_{84}N_2O_6$: C, 76.32; H, 9.61; N, 3.18. Found: C, 76.10; H, 9.80; N, 2.78.

Compound 6. Methanesulfonyl chloride (0.12 mL, 1.54 mmol) was added over 15 min to a mixture of **4** (330 mg, 0.390 mmol) and NEt_3 (0.260 mL, 2.12 mmol) in dry CH_2Cl_2 (5 mL) at −15 °C under N_2. After being stirred for 1 h at −15 °C, the reaction mixture was poured into a mixture of crushed ice (50 mL) and concentrated HCl (4 mL). The CH_2Cl_2 layer was separated, washed with saturated $NaHCO_3$ solution, dried (Na_2SO_4), and evaporated to give mesylate **5** (390 mg, ca. 80% pure, 0.35 mmol) as an oil. Crude **5** (170 mg, ca. 0.15 mmol), 4,4′-dihydroxy-2,2′-bipyridine (11.8 mg, 60.0 μmol), K_2CO_3 (50.0 mg, 362 μmol), and ^{n}Bu$_4$NI (2 mg, 6 μmol) were stirred vigorously in ethyl acetate (500 μL) and water (500 μL) at 60 °C for 20 h. Water (20 mL) was added, and the mixture was extracted three times with ethyl acetate (20 mL). The combined organic layers were dried ($MgSO_4$) and evaporated. Preparative chromatography (silica, CH_2Cl_2/MeOH 10:1) yielded **6** as a white powder (49.2 mg, 27.1 μmol, 44.0%). Chart 2 shows the structures of **4**−**6**. ^{1}H NMR (500 MHz, $CDCl_3$, 25 °C): δ 8.50 (d, J = 5.7 Hz, 2H, H^{6A}), 8.14 (s br, 2H, H^{3A}), 6.93 (dd, J = 5.5, 2.1 Hz, 2H, H^{5A}), 6.71 (d, J = 2.1 Hz, 4H, H^{2B}), 6.60 (t, J = 2.2 Hz, 2H, H^{4B}), 6.56 (d, J = 2.2 Hz, 8H, H^{2C}), 6.41 (t, J = 2.2 Hz, 4H, H^{4C}), 5.18 (s, 4H, $H^{OCH_2-ringB}$), 4.97 (s, 8H, $H^{OCH_2-ringC}$), 3.94 (t, J = 6.6 Hz, 16H, $H^{OCH_2CH_2}$), 1.77 (tt, J = 7.3, 6.6 Hz, 16H, $H^{OCH_2CH_2}$), 1.45 (tt, J = 7.5, 7.3 Hz, 16H, $H^{OCH_2CH_2CH_2}$), 1.29−1.38 (m, 64H, $H^{octyl(CH_2)_4}$), 0.89

(9) Constable, E. C. *Metals and Ligand Reactivity*; VCH: Weinheim, Germany, 1996; Chapter 2.
(10) Abdel-Mottaleb, M. M. S.; Schuurmans, N.; De Feyter, S.; van Esch, J.; Feringa, B. L.; De Schryver, F. C. *Chem. Commun.* **2002**, 1894−1895.
(11) Hawker, C. J.; Fréchet, J. M. J. *J. Am. Chem. Soc.* **1990**, *112*, 7638−7647.
(12) Widmer, I.; Huber, U.; Stöhr, M.; Merz, L.; Güntherodt, H.-J.; Hermann, B. A.; Samorí, P.; Rabe, J. P.; Rheiner, P. B.; Creiveldinger, G.; Murer, P. *Helv. Chim. Acta* **2002**, *85*, 4255−4263.
(13) Wu, P.; Fan, Q.; Deng, G.; Zeng, Q.; Wang, C.; Bai, C. *Langmuir* **2002**, *18*, 4342−4344.
(14) Prokhorova, S. A.; Sheiko, S. S.; Mourran, A.; Azumi, R.; Beginn, U.; Zipp, G.; Ahn, C. H.; Holerca, M. N.; Percec, V.; Möller, M. *Langmuir* **2000**, *16*, 6862−6867.
(15) Wu, P.; Fan, Q.; Zeng, Q.; Wang, C.; Deng, G.; Bai, C. *ChemPhysChem.* **2002**, 633−637.
(16) Constable, E. C.; Hermann, B. A.; Housecroft, C. E.; Merz, L.; Scherer, L. J. *Chem. Commun.* **2004**, 928−929.
(17) Case, F. H. *J. Org. Chem.* **1962**, *27*, 640−641.
(18) Forier, B.; Dehaen, W. *Tetrahedron* **1999**, *55*, 9829−9846.
(19) Ichinose, K.; Ebizuka, Y.; Sankawa, U. *Chem. Pharm. Bull.* **2001**, *49*, 192−196.
(20) Patrick, D. L.; Cee, V. J.; Beebe, T. P., Jr. *Science* **1994**, *265*, 231−234.
(21) Scheuring, S.; Ringler, P.; Borgnia, M.; Stahlberg, H.; Müller, D. J.; Agre, P.; Engel, A. *EMBO J.* **1999**, *18*, 4981−4987.

Chart 2

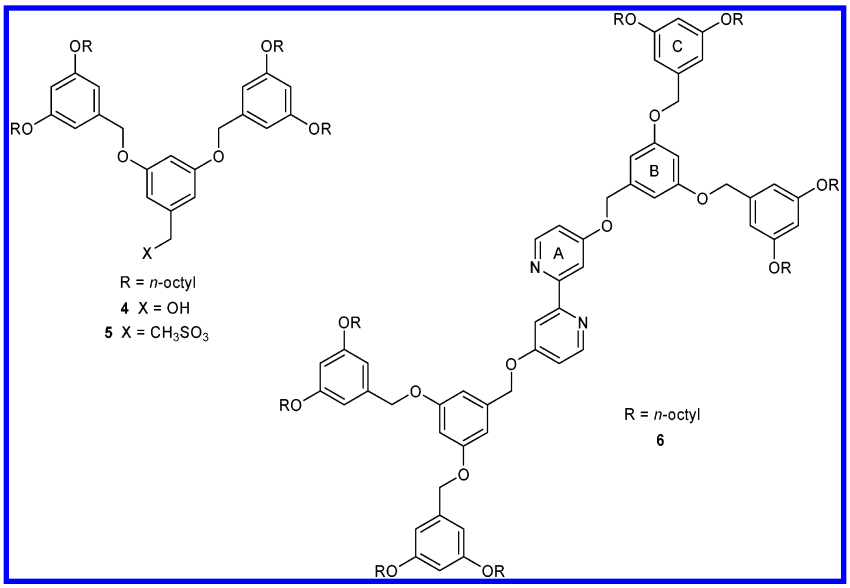

Chart 3

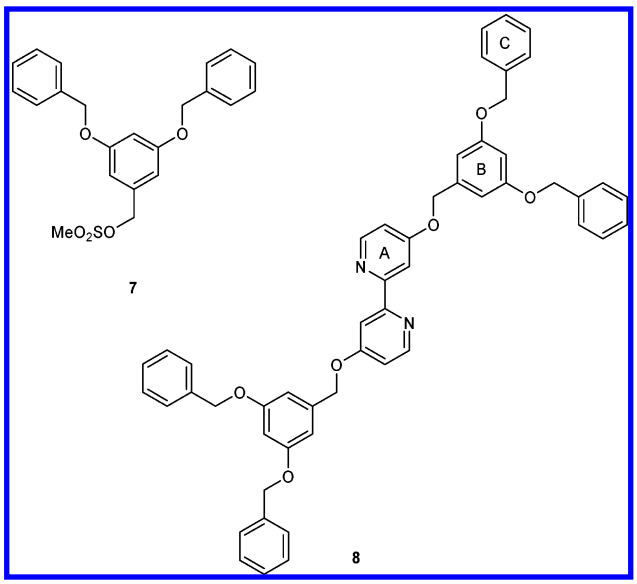

(t, J = 6.9 Hz, 24H, H^{CH_3}). ^{13}C NMR (125 MHz, $CDCl_3$, 25 °C): δ 166.2, 160.7, 160.3, 157.2, 150.0, 139.0, 138.1, 112.0, 107.5, 106.6, 105.8, 102.1, 101.0, 70.3, 70.1, 68.2, 32.0, 29.5, 29.4, 29.4, 26.2, 22.8, 14.2. IR (neat): $\bar{\nu}$ (cm^{-1}) 2924 m, 2854 m, 1589 s, 1450 s, 1373 m, 1157 s, 1049 s, 825 m. MS (MALDI+): m/z 1818.7 $[M]^+$, 1880.6 [M + Na + K]$^+$. UV/vis (CH_2Cl_2): λ/nm (ϵ/M^{-1} cm^{-1}) 276 (37 200). Anal. Calcd for $C_{116}H_{172}N_2O_{14}$: C, 76.61; H, 9.53; N, 1.54. Found: C, 76.07; H, 9.37; N, 1.76.

Compound 8. Crude mesylate **7** (see Chart 3, 400 mg, ca. 80% pure, 800 μmol), 4,4′-dihydroxy-2,2′-bipyridine (60.0 mg, 305 μmol), K_2CO_3 (240 mg, 1.74 mmol) and $^nBu_4NI$ (10 mg, 30 μmol) were stirred vigorously in ethyl acetate (1 mL) and water (1 mL) at room temperature for 20 h. Water (20 mL) was added, and the mixture was extracted three times with ethyl acetate (20 mL). The combined organic layers were dried (Na_2SO_4) and evaporated. Chromatography over silica (CH_2Cl_2/MeOH 15:1) yielded **8** as a white powder (82.5 mg, 104 μmol, 34.7%). ^1H NMR (500 MHz, $CDCl_3$, 25 °C, $CHCl_3$): δ 8.48 (d, J = 5.7 Hz, 2H, H^{6A}), 8.06 (d, J = 2.4 Hz, 2H, H^{3A}), 7.42 (d, J = 7.1 Hz, 8H, H^{2C}), 7.37 (dd, J = 7.6 Hz, 7.6 Hz, 8H, H^{3D}), 7.32 (dd, J = 7.3 Hz, 7.1 Hz, 4H, H^{4C}), 6.89 (dd, J = 5.6, 2.5 Hz, 2H, H^{5A}), 6.70 (d, J = 2.1 Hz, 4H, H^{2B}), 6.60 (t, J = 2.2 Hz, 2H, H^{4B}), 5.16 (s, 4H, $H^{OCH_2-ringB}$), 5.05 (s, 8H, H^{OCH_2Ph}). ^{13}C NMR (125 MHz, $CDCl_3$, 25 °C, $CHCl_3$): δ 165.9, 160.4, 158.0, 150.4, 138.3, 136.8, 128.8, 128.2, 127.7, 111.7, 107.3, 106.6, 102.0, 70.3, 69.9. IR (neat): $\bar{\nu}$ (cm^{-1}) 3032 w, 2901 w, 2870 w, 1967 w, 1875 w, 1736 w, 1590 s, 1443 m, 1373 m, 1296 s, 1149 s, 1027 s, 864 m, 825 s, 733 m, 694 s. MS (ESI+): m/z 793 $[M]^+$). Anal. Calcd. for $C_{52}H_{44}N_2O_6 \cdot 2H_2O$: C, 75.34; H, 5.86; N, 3.38. Found: C, 75.56; H, 5.67; N, 3.05.

[Pd(3)Cl$_2$]. Compound **3** (35 mg, 39 μmol) and $K_2[PdCl_4]$ (13 mg, 40 μmol) were refluxed in ethanol (20 mL) for 16 h. The solvent was evaporated, hexanes were added to the yellow residue, and the resultant suspension was filtered through Celite to give a yellow filtrate. The solvent was evaporated to give [Pd(**3**)Cl_2] as a yellow oil (41 mg, 39 μmol, 98%). ^1H NMR (500 MHz, $CDCl_3$, 25 °C): 8.62 (d, J = 6.7 Hz, 2H, H^{6A}), 7.66 (d, J = 2.6 Hz, 2H, H^{3A}), 6.77 (dd, J = 6.7, 2.6 Hz, 2H, H^{5A}), 6.62 (d, J = 2.2 Hz, 4H, H^{2B}), 6.43 (t, J = 2.2 Hz, 2H, H^{4B}), 5.32 (s, 4H, $H^{OCH_2-ringB}$), 3.94 (t, J = 6.6 Hz, 8H, $H^{OCH_2CH_2}$), 1.74 (tt, J = 6.8, 6.5 Hz, 8H, $H^{OCH_2CH_2}$), 1.42 (tt, J = 7.5, 7.3 Hz, 8H, $H^{OCH_2CH_2CH_2}$), 1.25−1.37 (m, 32H, $H^{octyl(CH_2)_4}$), 0.88 (t, J = 7.0 Hz, 12H, H^{CH_3}). ^{13}C NMR (125 MHz, $CDCl_3$, 25 °C): δ 167.2, 160.8, 157.2, 150.8, 136.4, 113.1, 110.3, 106.3, 101.6, 71.8, 68.3, 31.8, 29.4, 29.3 (two overlapping signals), 26.1, 22.7, 14.1. IR (neat): $\bar{\nu}$ (cm^{-1}) 2924 s, 2854 m, 1736 m, 1605 s, 1450 m, 1335 m, 1219 w, 1165 s, 1041 m, 841 m, 764 m. MS (FAB): m/z 985 $[M - 2Cl]^+$; UV/vis (CH_2Cl_2): λ/nm (ϵ/M^{-1} cm^{-1}) 301 (10 000), 289 (9800). Anal. Calcd for $C_{56}H_{84}Cl_2N_2O_6Pd$: C, 63.54; H, 8.00; N, 2.65. Found: C, 63.90; H, 8.09; N, 2.42.

[Pd(3)$_2$][PF$_6$]$_2$. [Pd(**3**)Cl_2] (38.0 mg, 35.9 μmol), compound **3** (31.6 mg, 35.9 μmol), and $TlPF_6$ (26.2 mg, 75 μmol) were stirred in dichloromethane (20 mL) at room temperature for 4 h. The suspension was filtered through Celite, and the solvent of the filtrate was evaporated. Sonicating in MeOH (15 mL) for 2 min afforded [Pd(**3**)$_2$]-$[PF_6]_2$ as a pale yellow powder (68.0 mg, 31.5 μmol, 87.7%). ^1H NMR (500 MHz, CD_2Cl_2, 25 °C, CH_2Cl_2): 8.38 (d, J = 6.8 Hz, 4H, H^{6A}), 7.69 (d, J = 2.1 Hz, 4H, H^{3A}), 7.50 (br s, 4H, H^{5A}), 6.58 (d, J = 2.2 Hz, 8H, H^{2B}), 6.42 (t, J = 2.1 Hz, 4H, H^{4B}), 5.27 (s, 8H, $H^{OCH_2-ringB}$), 3.92 (t, J = 6.5 Hz, 16H, $H^{OCH_2CH_2}$), 1.73 (tt, J = 6.7, 6.5 Hz, 16H, $H^{OCH_2CH_2}$), 1.42 (tt, J = 7.5, 6.7 Hz, 16H, $H^{OCH_2CH_2CH_2}$), 1.23−1.37 (m, 64H, $H^{octyl-(CH_2)_4}$), 0.87 (t, J = 7.1 Hz, 24H, H^{CH_3}). ^{13}C NMR (125 MHz, CD_2Cl_2, 25 °C): δ 168.7, 160.8, 157.2, 151.8, 135.9, 114.3, 111.6, 105.9, 101.5, 72.1, 68.2, 31.8, 29.3, 29.2, 29.2, 26.0, 22.6, 13.9. IR (neat): $\bar{\nu}$ (cm^{-1}) 2924 s, 2854 m, 1605 s, 1443 m, 1335 m, 1227 w, 1165 s, 1041 m, 825 s, 687 m. MS (ESI+): m/z 2012.3 $[M - PF_6]^+$, 933.3 $[M - 2PF_6]^{2+}$; UV/vis (CH_2Cl_2) λ/nm (ϵ/M^{-1} cm^{-1}): 288

(27 700), 236 (92 400). Anal. Calcd for $C_{112}H_{168}F_{12}N_4O_{12}P_2Pd$: C, 62.31; H, 7.84; N, 2.60. Found: C, 63.38; H, 7.80; N, 3.05.

Crystal Data for Compound 8. Data were collected on an Enraf Nonius Kappa CCD instrument; for data reduction, solution, and refinement we used the programs COLLECT,[22] SIR97,[23] and CRYSTALS (version 12).[24] Crystal data: $C_{158}H_{134}Cl_6N_6O_{18}$ ($3C_{52}H_{44}N_2O_6 \cdot 2CHCl_3$), $M = 2617.55$, triclinic, space group $P\bar{1}$, $a = 12.7464(2)$, $b = 15.0932(2)$, $c = 18.6957(3)$ Å, $\alpha = 95.3241(7)$, $\beta = 95.2033(7)$, $\gamma = 108.0007(7)°$, $U = 3378.78(9)$ Å^3, $Z = 1$, $D_c = 1.286$ Mg m^{-3}, μ(Mo Kα) = 0.197 mm^{-1}, $T = 173$ K. Reflections collected = 16 039; refinement of 9188 reflections (883 parameters) with $I > 1.5\sigma(I)$ converged at final $R1 = 0.0659$, $wR2 = 0.0786$.

Results

Compound Synthesis and Single-Crystal Structure of Compound 8. The synthetic strategy adopted was the reaction of a nucleophilic bpy derivative 4,4′-dihydroxy-2,2′-bipyridine[17] with an electrophilic dendritic wedge. The first-generation mesylate wedge **2**[18,19] was prepared in 80% yield by mesylation of the benzyl alcohol **1**[11,25−27] under standard reaction conditions. This first-generation dendritic wedge was coupled with 4,4′-dihydroxy-2,2′-bipyridine under phase-transfer conditions (^{n}Bu$_4$NI, ethyl acetate−water) in the presence of K_2CO_3 to give the first-generation (G1) ligand **3** in 74% yield. A related ligand with a different spacer between the bpy domain and the wedge has been reported by Vögtle et al.[28] Compound **3** was characterized by routine techniques. The major peaks in the electrospray mass spectrum were assigned to $[M + H]^+$ and $[M + Na]^+$. Signals in the ^{1}H NMR spectrum were assigned by COSY methods. The solution room temperature ^{1}H NMR spectrum was sharp and well-resolved and indicated that rotation about the C−C and C−O single bonds is unhindered.

The second-generation mesylate wedge, **5**, was prepared from the corresponding alcohol **4**[25] by a strategy analogous to the first-generation wedge. Compound **5** was coupled to 4,4′-dihydroxy-2,2′-bipyridine to give **6** under the same phase transfer conditions as when **2** was converted to **3**. Compound **6** was obtained as a white powder in 44% yield and was characterized by ^{1}H (COSY) and ^{13}C NMR and UV−vis spectroscopies, mass spectrometry, and elemental analysis. Of particular note was the fact that the signal assigned to the two bipyridine protons H^{3A} was broad, in contrast to the well-resolved signal observed for H^{3A} in the first-generation analogue **3**. Other signals in the ^{1}H NMR spectrum of **6** were sharp and well-resolved. We attribute this phenomenon to hindered rotation about the inter-ring C−C bond in the bipyridine unit arising from the increased steric requirements of the second-generation wedge.

In parallel with our studies of monolayers, we are continuing to investigate solution- and solid-state structural properties of related molecular systems. Compound **8** was prepared in ∼35% yield by the same methodology as compound **6**, and its structure has been determined by single-crystal X-ray diffraction. The triclinic unit cell contains two independent fragments: one complete molecule is noncentrosymmetric, and the second is located on the center of symmetry. Figure 1 shows the structure of the noncentrosymmetric molecule. In both molecules, the bipyridine unit adopts the expected trans conformation with the two pyridine rings coplanar (dihedral angle between least squares planes is 2°). Also in both molecules, the two inner benzyl substituents adopt syn conformations with respect to the bpy unit (see Chart 4). The outer benzyl groups adopt syn and anti conformations with respect to the C^4 proton (Chart 4). A search of all aromatic ethers in the Cambridge Crystallographic Database indicates a strong preference for the $COCH_2C$ residue to lie in the plane of the attached aromatic ring. In compound **8**, these torsion angles lie in the range 1.0−20.8° for the two different molecules; the dihedral angles between the least squares planes of adjacent pairs of pyridine−benzyl or benzyl−benzyl rings lie in the range 4.2−88.2°. These metrical data, in particular the angular information relating to the ether groups, provide valuable supporting evidence for the conformational analysis that follows.

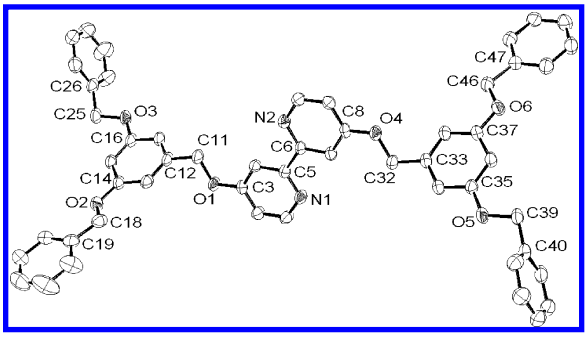

Figure 1. Solid-state structure of the noncentrosymmetric molecule of compound **8** present in the unit cell. For clarity, hydrogen atoms are omitted and selected atoms only are numbered. Important bond lengths and angles: N(1)−C(5) = 1.342(3), N(2)−C(6) = 1.343(3), C(5)−C(6) = 1.491(3), O(1)−C(3) = 1.368(3), O(1)−C(11) = 1.433(3), O(2)−C(14) = 1.369(3), O(2)−C(18) = 1.432(3), O(3)−C(16) = 1.372(3), O(3)−C(25) = 1.440(3), O(4)−C(8) = 1.363(3), O(4)−C(32) = 1.440(3), O(5)−C(35) = 1.368(3), O(5)−C(39) = 1.441(3), O(6)−C(37) = 1.374(3), O(6)−C(46) = 1.430(3) Å; C(3)−O(1)−C(11) = 116.6(2), C(14)−O(2)−C(18) = 116.7(2), C(16)−O(3)−C(25) = 117.2(2), C(8)−O(4)−C(32) = 116.5(2), C(35)−O(5)−C(39) = 117.3(2), C(37)−O(6)−C(46) = 116.7(2)°. The other molecule in the unit cell has similar bond lengths and angles.

Chart 4. Conformations (syn and anti) of the Benzyl Groups Are Defined (a) with Respect to the Interannular C−C Bond of the bpy Unit or (b) with Respect to the C^4−H Bond of a Phenyl Ring

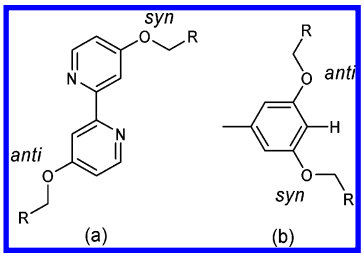

Imaging the First- and Second-Generation Dendrons 3 and 6. Good quality and extensive self-organized monolayers of **3** were obtained upon allowing solutions in volatile solvents to evaporate under ambient conditions. Although some regions of multilayers and apparently amorphous material are obtained, this method of solution casting has, in our hands, proved to be

(22) *Collect* Software; Bruker Nonius BV: Delft, The Netherlands, 1997−2001.
(23) Altomare, A.; Burla, M. C.; Camalli, M.; Cascarano, G. L.; Giacovazzo, C.; Guagliardi, A.; Grazia, A.; Moliterni, G.; Polidori, G.; Spagna, R. *J. Appl. Crystallogr.* **1999**, *32*, 115−119.
(24) Betteridge, P. W.; Carruthers, J. R.; Cooper, R. I.; Prout, K.; Watkin, D. J. *J. Appl. Crystallogr.* **2003,** *36*, 1487−1487.
(25) Rheiner, P. B.; Seebach, D. *Chem.−Eur. J.* **1999**, *5*, 3221−3236.
(26) Nierengarten, J.-F.; Felder, D.; Nicoud, J.-F. *Tetrahedron Lett.* **1999**, *40*, 269−272.
(27) Felder, D.; Nava, M. G.; Carreon, M. D. P.; Eckert, J.-F.; Luccisano, M.; Schall, C.; Masson, P.; Gallani, J.-L.; Heinrich, B.; Guillon, D.; Nierengarten, J.-F. *Helv. Chim. Acta* **2002**, *85*, 288−319.
(28) Vögtle, F.; Plevoets, M.; Nieger, M.; Azzelini, G. C.; Credi, A.; De Cola, L.; De Marchis, V.; Venturi, M.; Balzani, V. *J. Am. Chem. Soc.* **1999**, *121*, 6290−6298.

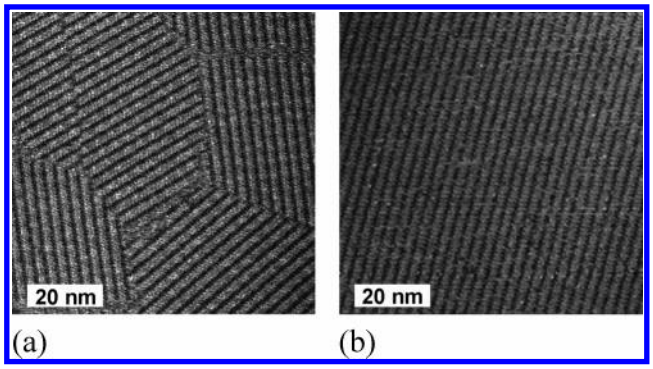

Figure 2. STM image of a monolayer of **3** on HOPG formed (a) from dichloromethane solution (80 nm × 80 nm, $U_b = -700$ mV, $I_t = 8$ pA) and (b) from hexane solution (80 nm × 80 nm, $U_b = -700$ mV, $I_t = 10$ pA). In image (a), different small domains can be seen; image (b) shows part of a domain extending over more than 500 nm × 500 nm.

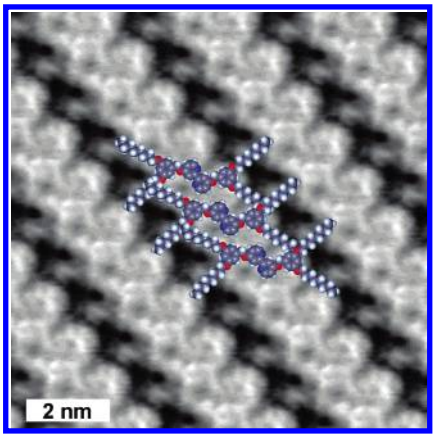

Figure 3. STM image of a monolayer of **3** formed from hexane solution on HOPG (10 nm × 10 nm, averaged over 41 positions, $U_b = -900$ mV, $I_t = 40$ pA). The benzyl groups have the highest intensity. Molecular models of **3** showing the best-fit conformation are also shown; this is discussed later in the article.

a reliable and reproducible method for obtaining monolayers with large homogeneous domains. In STM images of self-organized monolayers of molecule **3** (Figure 2a), we observed multiple domain formation with a lamellar arrangement. The individual domain sizes ranged from some 50 nm × 50 nm up to 1000 nm × 1000 nm depending on the exact preparation conditions. While on first sight the orientations of domains in Figure 2a appear to reflect the threefold symmetry of the frontier orbitals of the graphite surface (the sixfold symmetry of single graphite layer is reduced to threefold as a consequence of A−B−A stacking of the layers in α-graphite[29]), a detailed analysis reveals the additional presence of small angle domain boundaries (see the following discussion).

We prepared these multiple domains from hexane and dichloromethane solutions. Those from hexane were typically and reproducibly of much larger size than those from dichloromethane (Figure 2). This is consistent with a slower rate of evaporation of hexane (bp 342 K, $\Delta_{vap}H° = 31.56$ kJ mol^{-1}) than dichloromethane (bp 313 K, $\Delta_{vap}H° = 28.82$ kJ mol^{-1}). Figure 3 shows an enlargement of a monolayer of **3** obtained from hexane solution. The high-resolution images that we were able to obtain at room temperature in air (for example, that shown in Figure 3) display submolecular resolution approaching the atomic level. With such weakly physisorbed molecules, very low tunneling currents have to be used in order not to destroy the self-organized monolayers. Despite this, we obtained remarkably high-resolution images.

We regularly observed these two sets of three domains with a reproducible small angle relationship between the sets of 6.5° (Figure 4a). In the high-resolution image in Figure 4a, the two peripheral benzyl groups of molecule **3** appear as regions of highest intensity, consistent with the occupied frontier orbitals being localized on these sites. The contrast in STM images of organic molecules has often been successfully compared to the frontier orbitals, either the HOMO or LUMO, according to the polarity of the applied potential.[30,31] Semiempirical calculations at the PM3 level[32] confirmed that the highest filled orbitals of **3** are located on the benzyl substituents and extend to the oxygen atoms. The occupied orbitals localized on the central bpy unit have a slightly lower energy. In the STM images of **3**, the bipyridine rings are harder to identify than the benzyl groups. A detailed analysis is described later in this article and allows a clear identification of the molecular conformation. Parts b and c of Figure 4 were obtained by averaging a 10 nm × 10 nm window over 121 and 104 positions for the left and right domains shown in Figure 4a, respectively. STM image appearance is dependent on different scanning parameters, tips, and orientation relative to the scanning direction. Indeed, a comparison of Figures 3 and 4 shows differences in resolution. This is due to a different tip and a difference in the orientation of the molecules, which only becomes apparent when the images are examined in detail. Differences between parts b and c of Figure 4 cannot be a consequence of instrumental technique since the two figures are enlargements of the *same* image. Two differences between parts b and c of Figure 4 are apparent: (i) the alignment of the individual molecules within the rows and (ii) different "internal" structure of the molecules. We can quantify these differences by measuring an angle θ that is the internal angle between two lines defined by connecting the two benzyl groups (i.e., seen as the bright spots) of one molecule and connecting two benzyl groups of adjacent molecules (see parts b and c of Figure 4). We discuss these differences in terms of anti,syn and anti,anti conformations of molecules of **3** later in the article.

Evaporation of solutions of the second-generation compound **6** also gave good quality monolayers in which multiple domains were observed. Figure 5 depicts the STM images of two domains showing a slightly different arrangement of the rows and different internal structure of the molecules. For these images, the averaging analysis of the upper and lower domains in Figure 5a was performed over 62 and 44 positions, respectively, allowing the identification of single molecules almost without further interpretation. In the upper domain (Figure 5b), the molecule is stretched in an X-like configuration. However, in the lower domain (Figure 5c), molecule **6** clearly adopts a different conformation on the graphite surface. In contrast to **3**, the second-generation compound **6** does not form lamellar stripes. The bipyridine rings of molecule **6** are imaged with

(29) Lim, R.; Li, J.; Li, S. F. Y.; Feng, Z.; Valiyaveettil, S. *Langmuir* **2000**, *16*, 7023−7030.
(30) Miura, A.; Chen, Z.; Uji-I, H.; De Feyter, S.; Zdanowska, M.; Jonkheijm, P.; Schenning, A. P. H. J.; Meijer, E. W.; Würthner, F.; De Schryver, F. C. *J. Am. Chem. Soc.* **2003**, *125*, 14968−14969.
(31) Qiu, X.; Wang, C.; Yin, S.; Zeng, Q.; Xu, B.; Bai C. *J. Phys. Chem. B* **2000**, *104*, 3570−3574.
(32) Calculations were made using the PM3 implementation in Spartan '04, Wavefunction Inc.: Irvine, CA, 2003.

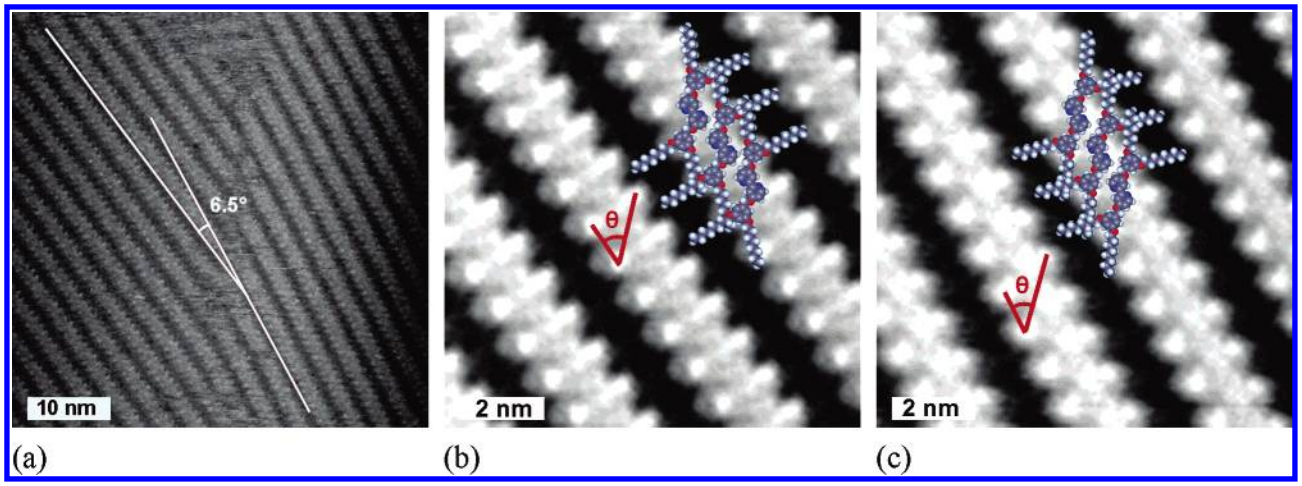

Figure 4. (a) STM images of two domains of monolayers of **3** on HOPG. The angle difference between the two domains is 6.5°. (b) and (c) Expanded images (10 nm × 10 nm) of the left and right domains, respectively, of (a). Panel (b) corresponds to conformation *anti,anti*-**3** ($\theta = 55°$), and panel (c) corresponds to conformation *anti,syn*-**3** ($\theta = 38°$) (see Chart 4 and later discussion). Scan parameters: 50 nm × 50 nm, $U_b = -1111$ mV, $I_t = 15$ pA.

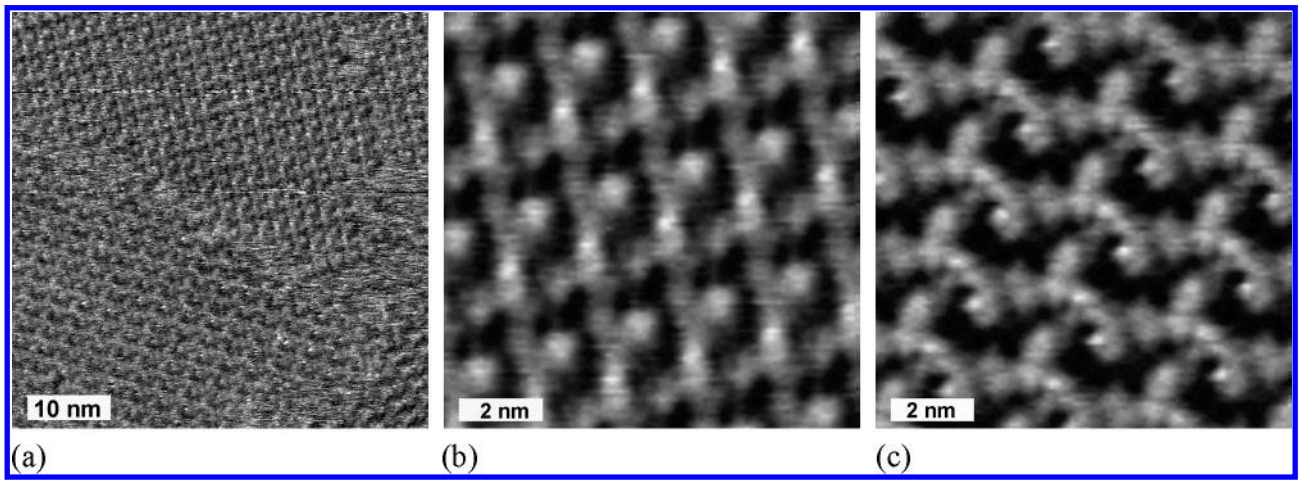

Figure 5. (a) STM images of two domains of monolayers of **6** on HOPG (50 nm × 50 nm. (b) and (c) Expanded images (10 nm × 10 nm) of the upper and lower domains, respectively, of (a). Scan parameters: $U_b = -1111$ mV, $I_t = 15$ pA.

higher contrast than those in molecule **3**, and this allows a straightforward interpretation of the structure of monolayers of **6** since all of the aromatic rings are directly observed.

Switching Molecular Conformation. Large dendritic substituents are expected to impose a significant mechanical barrier to conformational change involving the bpy unit when the molecule is constrained on a surface. In particular, the conformational change from the trans arrangement of nitrogen atoms in a free ligand to the cis conformation within a coordinated ligand is expected to have a high activation barrier associated with both the mechanical motion of the dendritic substituents and the necessary involvement of nonplanar bpy which cannot lie flat on the surface during the conformational change. Despite this, we attempted to address the conformation of the bpy domain of molecule **3** through interaction with metal ions or protons, both of which result in the formation of cis species under solution and normal solid-state conditions.[33] Treating the adsorbed monolayer of **3** with dilute aqueous solutions of metal salts (copper(II) sulfate or palladium(II) acetate) destroyed the ordered domains. After such treatment, no organized monolayers were observed with STM. The complexes $[Pd(\mathbf{3})_2][PF_6]_2$ and $[Pd(\mathbf{3})Cl_2]$ were prepared from **3**. These complexes contain square planar PdN_4 and PdN_2Cl_2 units, respectively, which are expected to interact optimally with the graphite surface. However, treatment of a graphite surface with hexane solutions of either of these complexes did not result in the formation of ordered monolayers. Treating the monolayers of **3** with aqueous acidic solutions (0.1 M HCl or 0.1 M AcOH) did not influence the structure of the monolayers, which were imaged unchanged after this treatment. However, passing gaseous HCl over the monolayers resulted in a conformational change of all molecules in small domains, and the formation of a highly ordered structure with new periodic properties (Figure 6). The molecules are no longer stacked side by side in a trans conformation, forming lamellar stripes as in Figure 3. In contrast, the domains in the protonated system are built from large X-like structures. In many hundreds of recorded images of compound **3**, these X-shaped structures have never been observed, and we are confident that they are a result of the treatment with HCl. The smaller size of the domains makes them less stable for imaging. Drift in the images is frequently observed, and this makes it impossible to record images of the protonated monolayer of the quality used for the conformational analysis of **3**.

Although the protonation itself cannot be seen directly, the conformational change after treatment with HCl is dramatic and

(33) Constable, E. C. *Adv. Inorg. Chem.* **1989**, *34*, 1−63.

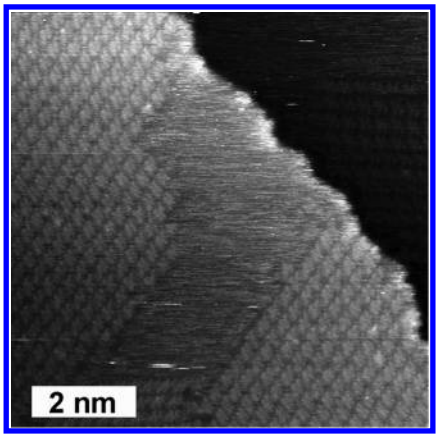

Figure 6. STM image of a monolayer of **3** on HOPG after treatment with gaseous HCl (80 nm × 80 nm, $U_b = -800$ mV, $I_t = 9$ pA). The ragged line running from top to bottom of the figure is a graphite step edge.

characteristic. Qualitative modeling and the known protonation chemistry of 2,2′-bipyridine are consistent with the molecule adopting a cis conformation. Even after treatment with gaseous HCl, some large domains in the monolayers retain a lamellar structure similar to that observed for unprotonated **3**. It is proposed that the cis domains are formed in a concerted conformational change in which a number of molecules in a domain change simultaneously. This conclusion follows from observations that (i) only small domains were observed and (ii) no domains showed mixtures of both cis and trans conformations. At this stage, we cannot speculate on the stoichiometry of the protonated species, but offer these preliminary results as an indication of the use of the STM to monitor chemical changes within a self-organized monolayer.

Data Analysis and Discussion

While the analysis of pattern formation in STM images of self-organized monolayers is at a very advanced stage,[4−6] studies including conformational analysis of flexible molecules are still scarce.[34−37] There are several factors responsible for this. Usually, very high resolution images are necessary to identify individual conformations, but these are often difficult to obtain with highly flexible molecules. Additionally, molecules with conformational freedom have to be designed carefully, if they are to form self-organized monolayers at all. Last, but not least, most high-resolution STM studies are still performed in ultrahigh vacuum with sublimed molecules; this is often impossible for large, flexible molecules. Many researchers refrain from measuring in air at room temperature because there are many more uncertainties, impurities, and thermal motion associated with the surface molecules. Thus, it remains a challenge to obtain high-resolution images under ambient conditions. The exclusion of measurement artifacts, errors due to drift, and averaging artifacts is very important. Also, reproducibility of experimental results is essential, as measurements of single events and molecules sometimes show noise (irregularities, etc.) and impurities on the same scale as the measured molecules. Errors

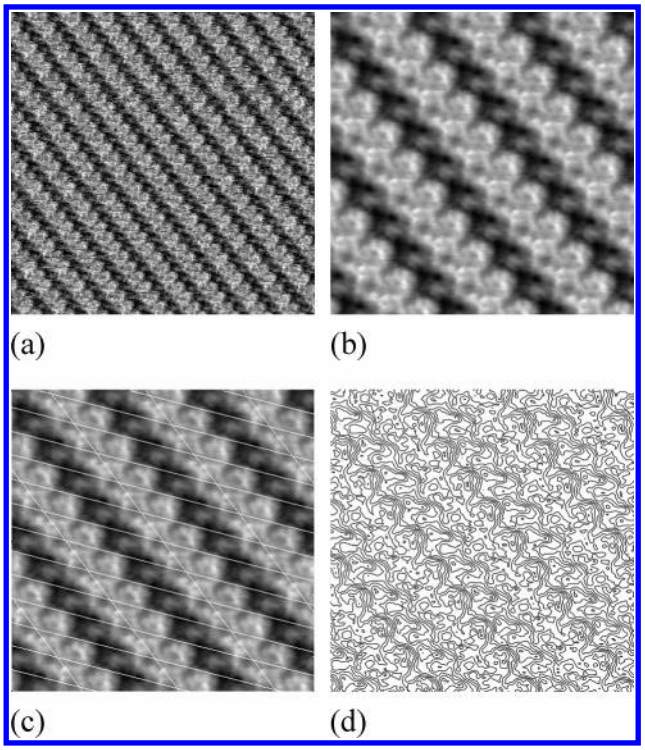

Figure 7. Process of data analysis of a measurement of a domain containing **3** after (a) flattening and (b) enlargement and averaging over 46 positions. Panel (c) shows overlaid unit cells and (d) shows a contour plot of (b). Scale: (a) 30 nm × 30 nm; (b)−(d) 10 nm × 10 nm.

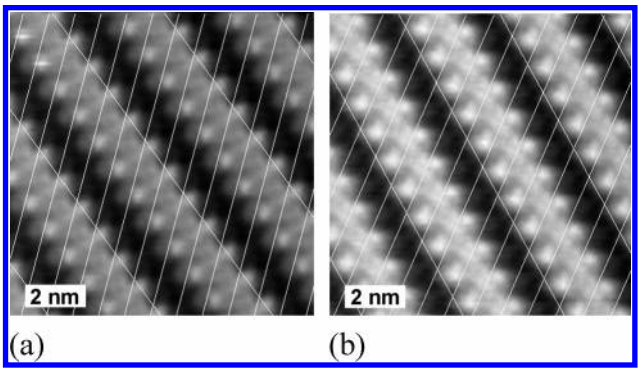

Figure 8. (a) and (b) Images from Figure 4, parts b and c, respectively, with their corresponding unit cells.

due to thermal drift of the apparatus can be excluded by carefully checking follow-up scans of the opposite slow scanning direction. Any compression or elongation due to drift is then easily recognized. A general observation in the STM images of our systems was that the domains were present from the first scan lines and remained very stable over time; no bleeding or migration was observed. Even though the monolayers were stable over time, they were very easily disturbed by scanning with tunneling currents above some 10 pA. In rare cases, a growth of domains was observed at the cost of unordered phases. Only measurements that meet the rigorous requirements listed above could be used for a successful conformational analysis.

We next describe in detail the process of conformational analysis for one example. Figure 7a shows the flattened (but otherwise raw) measurement of a monolayer of **3** on HOPG. The application of an averaging procedure (for details, see the Experimental Section) further reduces the random noise. Figure 7b shows an enlargement from Figure 7a that has been averaged

(34) Jung, T. A.; Schlittler, R. R.; Gimzewski, J. K. *Nature* **1997**, *386*, 696−698.
(35) Kim, K.; Plass, K. E.; Matzger, A. J. *Langmuir* **2003**, *19*, 7149−7152.
(36) Plass, K. E.; Kim, K.; Matzger, A. J. *J. Am. Chem. Soc.* **2004**, *126*, 9042−9053.
(37) Schuurmans, N.; Uji-I, H.; Mamdouh, W.; De Schryver, F. C.; Feringa, B. L.; van Esch, J.; De Feyter, S. *J. Am. Chem. Soc.* **2004**, *126*, 13884−13885.

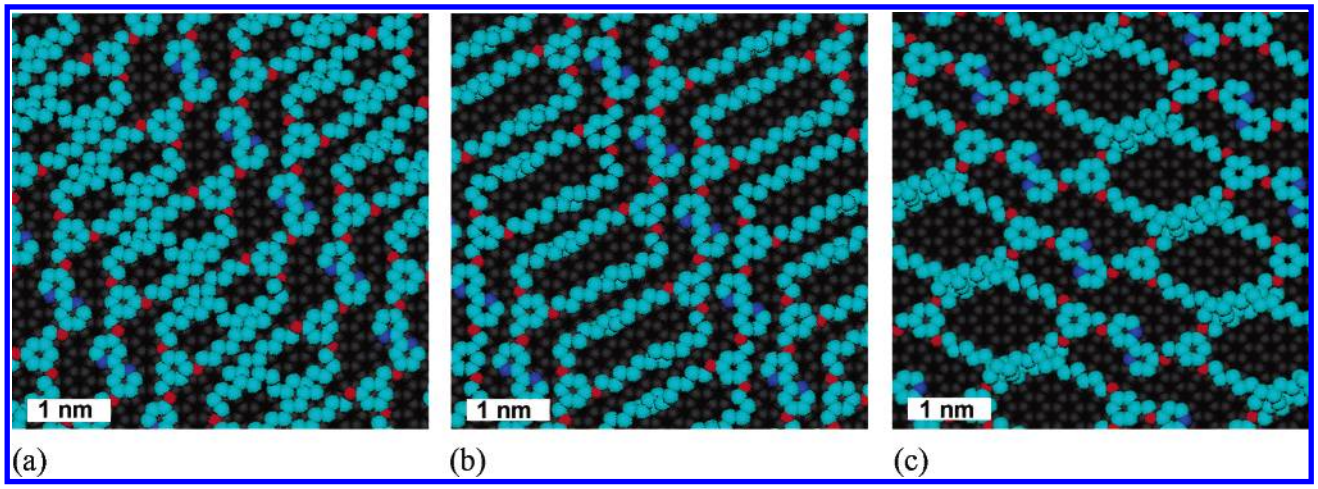

Figure 9. Molecular models of monolayers on graphite corresponding to the images shown in (a) Figure 4b, (b) Figure 4c, and (c) Figure 3. In the representations in this figure, the orientation of the graphite substrate is the same. The two-dimensional packing density is the same within experimental error.

Chart 5. Two Conformations of Compound **3** Observed in the STM Study

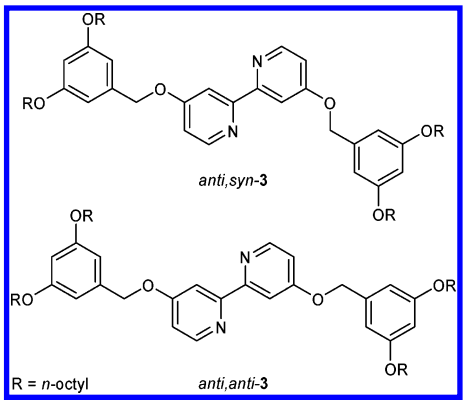

over 46 positions. The unit cell of the molecular layer can be deduced from a Fourier spectrum of an averaged image. One possible unit cell of the above measurement is shown in Figure 7c. The averaged image is printed with different contrast settings, and if needed, contour plots (Figure 7d) are printed as well. Molecular models of all relevant conformations were analyzed using computer graphics. The $C_{bpy}-O-C$ and $C_{benzyl}-O-C$ bond angles were constrained to the values observed crystallographically for compound **8** (117°) to reflect the π-component in the $C_{aromatic}-O$ bond. The models were overlaid on the STM images to find the best fits. Molecular orbital calculations were run on molecule **3** in different conformations to confirm that there was no significant change in either composition or relative ordering of the highest filled orbitals.

Following this analysis procedure, the unit cells, the molecular ordering, and the molecular conformation within the domains in Figures 3 and 4b,c could be identified. As the alkyl chains are insulating, and therefore hardly seen in STM images,[38,39] the following discussion is focused on the syn and anti conformations of the $ArOCH_2Ar$ groups. Two different conformations of **3** could be determined, and these are shown in Chart 5. In addition to this, the molecules were found in different assembly patterns. Figures 7c and 8a,b show the averaged images with their respective unit cells, and Figure 9 shows the proposed molecular arrangements. The unit cell dimensions (defined by the cell lengths a and b and the acute angle, α, in the rhombus) are $a = 3.8$ nm, $b = 1.1$ nm, $\alpha = 51°$ (Figures 8a and 9a), $a = 3.8$ nm, $b = 1.1$ nm, $\alpha = 52°$ (Figures 8b and 9b), and $a = 4.1$ nm, $b = 1.2$ nm, $\alpha = 38°$ (Figures 7c and 9c). This gives unit cell areas of 3.2, 3.3, and 3.0 nm^2, respectively. The alkane chains were not modeled, as they are not sufficiently resolved to be assigned with certainty. Nevertheless, the spacing between the molecules is exactly the right width for an arrangement in which all the octyl chains are in an extended conformation. It is assumed that they form an interdigitated pattern, thereby optimizing the two-dimensional crystallization energy. Only two of the possible conformations were found, but the anti,syn conformation at each B ring (Charts 1 and 4) was found at each side of molecule **3** as also found in the three-dimensional single-crystal X-ray structure of **8**. It is noteworthy that although the conformations and the molecular arrangements in Figure 9a−c are different, the two-dimensional packing density per molecule is roughly the same. In the domain of Figure 9c, the molecules are tilted much more along the row of molecules than for the other two domains shown.

The STM imaging measurements for the second-generation compound **6** proved to be more difficult than those of **3**. The monolayers of **6** are less stable than those of **3**, and it is more challenging to obtain images with a resolution as high as for the first-generation **3**. Nevertheless, most conformations could easily be excluded, and the conformation could be assigned with a high certainty. Figure 10 shows the observed molecular arrangements and conformations of **6** in the two different domains shown in Figure 5. In one domain (Figure 10a), the bpy unit is in a trans conformation (with respect to pyridine rings) and an anti,syn conformation (defined in Chart 4). The outer generation of benzyl groups attached to the inner-generation *anti*-benzyl group adopts an anti,syn conformation; the outer generation of benzyl groups attached to the *syn*-benzyl ring exhibits a syn,syn conformation (see Chart 4). In the other domain (Figure 10b), the benzyl groups attached to the bpy domain adopt an anti,anti conformation, while each pair of outer-generation benzyl groups adopts a syn,syn arrangement (Chart 4). At present, we are unable to say that these are the only conformations that are present in the monolayers of **6**.

(38) Rabe, J. P.; Buchholz, S. *Science* **1991**, *253*, 424−427.
(39) Cai, Y.; Bernasek, S. L. *J. Am. Chem. Soc.* **2004**, *126*, 14234−14238.

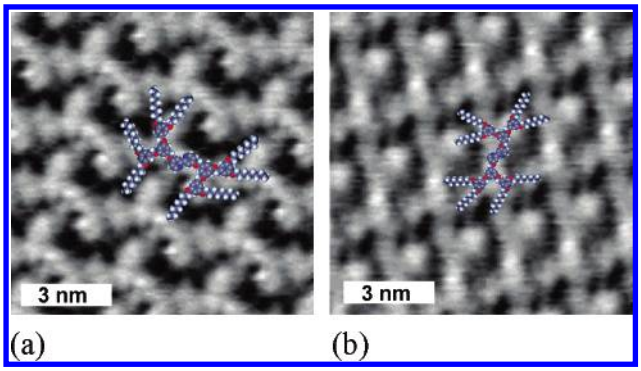

Figure 10. Expanded images (10 nm × 10 nm) of (a) the upper and (b) the lower domains, respectively, of Figure 5a. Overlaying the molecular structures confirms the two different conformations.

Conclusions

We have shown that deposition of a dendritic wedge functionalized ligand on a HOPG surface results in the formation of well-defined monolayers exhibiting different conformations of the molecule. The near-atomic resolution allows us to clearly assign two conformers. Both of them spontaneously and rapidly form molecular domains under ambient conditions. Within a molecular domain, only one conformer is present and domains of different conformers were observed side by side. No preference for one conformer was observed. Higher-generation dendrons attached to the bpy also showed at least two different conformers in self-organized monolayers.

Acknowledgment. This work was supported by the Swiss National Science Foundation under program NRP 47, the Portlandcementfabrik Laufen, and the University of Basel. We thank Prof. Dr. H.-J. Güntherodt for his continuous support and encouragement.

Supporting Information Available: Crystal data for compound **8** (CIF). This material is available free of charge via the Internet at http://pubs.acs.org.

JA043638+